Simulation study of InAlN/GaN high-electron mobility transistor with AlInN back barrier*

Tie-Cheng Han(韩铁成), Hong-Dong Zhao(赵红东)†, Lei Yang(杨磊), and Yang Wang(王杨)

School of Electronic and Information Engineering, Hebei University of Technology, Tianjin 300401, *China*

(Received 19 April 2017; revised manuscript received 24 June 2017; published online 20 August 2017)

In this work, we use a 3-nm-thick $Al_{0.64}In_{0.36}N$ back-barrier layer in $In_{0.17}Al_{0.83}N$/GaN high-electron mobility transistor (HEMT) to enhance electron confinement. Based on two-dimensional device simulations, the influences of $Al_{0.64}In_{0.36}N$ back-barrier on the direct-current (DC) and radio-frequency (RF) characteristics of InAlN/GaN HEMT are investigated, theoretically. It is shown that an effective conduction band discontinuity of approximately 0.5 eV is created by the 3-nm-thick $Al_{0.64}In_{0.36}N$ back-barrier and no parasitic electron channel is formed. Comparing with the conventional InAlN/GaN HEMT, the electron confinement of the back-barrier HEMT is significantly improved, which allows a good immunity to short-channel effect (SCE) for gate length decreasing down to 60 nm (9-nm top barrier). For a 70-nm gate length, the peak current gain cut-off frequency (f_T) and power gain cut-off frequency (f_{max}) of the back-barrier HEMT are 172 GHz and 217 GHz, respectively, which are higher than those of the conventional HEMT with the same gate length.

Keywords: InAlN/GaN HEMT, back barrier, electron confinement, short-channel effect (SCE)

PACS: 73.40.Kp, 85.30.Tv, 85.30.De **DOI:** 10.1088/1674-1056/26/10/107301

1. Introduction

The lattice-matched $In_{0.17}Al_{0.83}N$/GaN high-electron mobility transistors (HEMTs) show outstanding performances for high-frequency applications as a result of the congenital material advantages of the strain-free barrier layer and the large spontaneous polarization.[1–6] A major obstacle that limits the performances of $In_{0.17}Al_{0.83}N$/GaN HEMTs for further high-frequency operations is short-channel effect (SCE). Alternatively, since the SCE mainly originates from the poor electron confinement and the lack of the buffer isolation,[7] the insertion of a potential barrier such as an AlGaN[8–14] or an InGaN[15–18] at the backside of GaN channel is a good solution for suppressing SCE without excessively reducing top-barrier thickness.

Inserting a thin AlGaN layer between the channel and the buffer layer, an unwanted parasitic electron channel will be created at the GaN buffer layer.[8,11] In order to avoid the generation of the parasitic electron channel, an AlGaN buffer is adopted as a back-barrier, generally. However, growing high-quality AlGaN buffer layer is more difficult than GaN.[11,12] Meanwhile, the use of an AlGaN buffer instead of a GaN buffer also degrades the thermal conductivity of the structure.[10] Although an InGaN back-barrier seems to have no above-mentioned shortcomings, since the band gaps of InGaN are narrower than those of GaN, a thin parasitic electron channel is formed in the InGaN layer. Electrons in the InGaN well are hard to pinch off and deteriorate the device transconductance,[19] which is more pronounced for the ultrashort-gate device with a thick GaN channel and a relatively high indium composition(In$\sim$ 0.15).[17] In 2016, He *et al.* proposed the idea of using AlInN thin layer as a back-barrier,[19] which not only creates a barrier below the GaN channel, but also eliminates the parasitic electron channel. Therefore, this new back-barrier may have a great potential for further improving the performances of highly scaled devices.

In this work, we present an improved bottom confinement by applying a 3-nm-thick $Al_{0.64}In_{0.36}N$ back-barrier layer to short-gate InAlN/GaN HEMT. Two-dimensional device simulator (Silvaco Atlas)[20] is employed to calculate the band profile and the electron distribution of InAlN/GaN structure with or without an AlInN back-barrier. The influences of the AlInN back-barrier on the DC and RF characteristics of InAlN/GaN HEMT are investigated, theoretically. The results show that the AlInN back-barrier can effectively enhance the electron confinement, which can help InAlN/GaN HEMT to suppress the SCEs down to $L_G = 60$ nm (9-nm top barrier). A 70-nm-gate-length device with an AlInN back-barrier also has a distinct improvement in pinch-off quality and RF performance compared with the conventional HEMT.

2. Device description

In this work, the conventional InAlN/GaN heterostructure employed was epitaxially grown by metal–organic chemical vapor deposition (MOCVD) on a SiC substrate. The epitaxial structure consisted of a 2-μm undoped GaN buffer/channel layer, a 1-nm AlN interlayer and an 8-nm undoped $In_{0.17}Al_{0.83}N$ barrier layer. E-beam lithography was employed to define a 70-nm T-shape gate in the center of the 2-

*Project supported by the Natural Science Foundation of Hebei Province, China (Grant No. F2013202256).

†Corresponding author. E-mail: zhaohd@hebut.edu.cn

© 2017 Chinese Physical Society and IOP Publishing Ltd

μm source-drain space. A Ni/Au metal stack was deposited for the Schottky contact and had 2×40-μm gate width (W_g). The ohmic contacts were formed with a Si/Ti/Al/Ni/Au stack deposition and the contact resistance was $0.32\ \Omega\cdot$m. Finally, the device was passivated with SiN deposited by plasma-enhanced chemical vapor deposition (PECVD). The conventional heterostructure and experiment are described in detail in Ref. [6]. Compared with the conventional InAlN/GaN heterostructure, the newly proposed AlInN back-barrier heterostructure is assumed to add a 3-nm AlInN back-barrier layer below a 10-nm GaN channel layer as shown in Fig. 1.

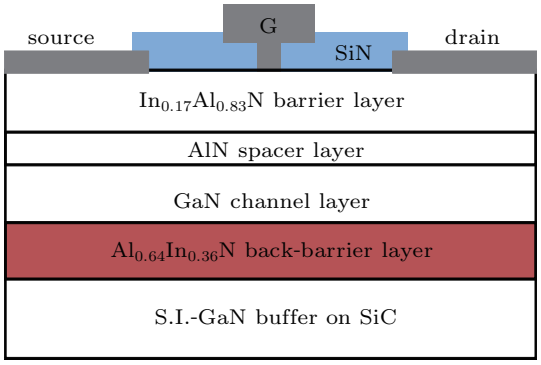


Fig. 1. (color online) Cross-sectional view of AlInN/AlN/GaN HEMT structure with $Al_{0.64}In_{0.36}N$ back-barrier.

Concerning the choice of Al composition for $Al_xIn_{1-x}N$ back-barrier material, we mainly consider the following principles.

(i) A negative polarization charge is induced at $Al_xIn_{1-x}N$ back-barrier/GaN buffer heterointerface to avoid forming parallel electron channel in GaN buffer;

(ii) A larger band gap than GaN to avoid forming a parasitic electron channel in $Al_xIn_{1-x}N$ back-barrier layer, i.e., $E_g > 3.42$ eV;

(iii) The back-barrier height induced by $Al_xIn_{1-x}N$ layer is highest.

By calculation, $Al_{0.64}In_{0.36}N$ meets the requirements. The models for calculating the relevant parameters are described in the next section.

3. Models and calibration

Due to the thermal effects that are not analyzed in this work, drift–diffusion transport model is invoked to complete the simulations, which can provide relatively fast simulation and an acceptable level of accuracy. Several important physical models such as polarizations, SRH, the low field electron mobility, and high field mobility are included in simulations.

The total polarization-induced sheet charge density for a top/bottom heterointerface is expressed as[21]

$$\begin{aligned}\sigma &= [P_{PE}(\text{bottom}) - P_{PE}(\text{top})] \\ &\quad + [P_{SP}(\text{bottom}) - P_{SP}(\text{top})],\end{aligned} \tag{1}$$

with

$$\begin{aligned}&P_{SP}(Al_xIn_{1-x}N) \\ &= -0.090x - 0.042(1-x) + 0.07x(1-x)\ \text{C/m}^2, \\ &P_{PE}(Al_xIn_{1-x}N/GaN) \\ &= -0.0525x + 0.148(1-x) + 0.0938x(1-x)\ \text{C/m}^2, \\ &P_{SP}(\text{GaN}) = -0.034\ \text{C/m}^2, \quad P_{SP}(\text{AlN}) = -0.090\ \text{C/m}^2.\end{aligned}$$

Here, P_{SP} and P_{PE} denote the spontaneous and piezoelectric polarizations respectively. In the real device, several effects (such as dislocations or the ambient condition) can reduce the polarization value. For calibration with the experimental data, we adopted the theoretical polarization value of 0.87 times as the simulation value.

In this work, we selected the following band gap calculation expression of $Al_xIn_{1-x}N$ material based on LDA-1/2 approach:[22]

$$E_g^{Al_xIn_{1-x}N} = xE(AlN) + (1-x)E(\text{InN}) - bx(1-x) \tag{2}$$

with

$$E(\text{AlN}) = 6.06\ \text{eV}, \quad E(\text{InN}) = 0.95\ \text{eV}, \quad b = 3.4x + 1.2.$$

The experimentally measured band offset at the AlN/GaN heterointerface is 1.42 eV.[23] The other band offsets of the top/bottom heterointerface rely on the relationship $\Delta E_{C,ABN} = 0.63\left[E_{gABN}(\text{top}) - E_{gABN}(\text{bottom})\right]$.[21] The physical parameters of materials in simulations are listed in Table 1.

Table 1. Parameters of GaN, AlN, and $Al_xIn_{1-x}N$ used in the simulation.

Parameter	GaN	AlN	$Al_{0.83}In_{0.17}N$	$Al_{0.64}In_{0.36}N$
Band gap/eV	3.42	6.15	4.62	3.44
Permittivity[21]	10.28	10.31	11.04	11.86
v_{sat} for electrons /10^7 cm·s^{-1}	2.0	2.17	1.1	0.1
Hole mobility/V$^{-1}\cdot$s$^{-1}\cdot$cm^2	22	14	82	100

The low-field mobility is modeled as follows:[20]

$$\begin{aligned}\frac{1}{\mu_0(T,N)} &= a\left(\frac{N}{N^{\text{ref}}}\right)\left(\frac{T}{300}\right)^{-1.5} \\ &\quad \times \ln\left[1 + 3\left(\frac{T}{300}\right)^2\left(\frac{N}{N^{\text{ref}}}\right)^{-2/3}\right] \\ &\quad + b\left(\frac{T}{300}\right)^{1.5} + \frac{c}{\exp(1065/T) - 1},\end{aligned} \tag{3}$$

where $\mu_0(T,N)$ is the mobility as a function of doping and lattice temperature. The values of the various parameters in Eq. (3) are given in Table 2.

Table 2. Low-field mobility model parameters for electron used in simulations.

T/K	N^{ref}/cm^{-3}	a/V·s·cm^{-2}	b/V·cm^{-2}	c/V·s·cm^{-2}
300	1×10^{17}	2.61×10^{-4}	9.8×10^{-4}	1.7×10^{-2}

The high-field mobility is modeled as follows:[20]

$$\mu(E) = \frac{\mu_0(T,N) + v_{\rm sat}\dfrac{E^{n_1-1}}{E_{\rm C}^{n_1}}}{1 + a_1\left(\dfrac{E}{E_{\rm C}}\right)^{n_2} + \left(\dfrac{E}{E_{\rm C}}\right)^{n_1}}, \tag{4}$$

where E and $v_{\rm sat}$ are the electric fields and saturation velocities. The values of $E_{\rm C}$, a_1, n_1, and n_2 are taken from Ref. [20].

The unintentional n-type doping concentration in each of the layers is assumed to be 1×10^{16} cm^{-3}. The donor states existing at the surface of barrier layer may be the main source of the electrons in the two-dimensional electron gas (2DEG).[24] Donor-like traps are introduced at the SiN/$In_{0.17}Al_{0.83}N$ interface with a single energy level of 0.42 eV below the conduction band and a density of 3.86×10^{13} cm^{-2}. Usually, additional p-type doping is used to compensate for unintentional n-type doping. We also consider acceptor-like traps in the GaN buffer with an energy level of 0.5 eV below the conduction band and a trap density of 5×10^{16} cm^{-3}. Using this setup, the simulated transfer characteristics (Fig. 2) and the 2DEG sheet density of the conventional HEMT show good agreement with the experimental results.[6] After the calibration, the simulations of InAlN/GaN HEMT with an AlInN back-barrier were carried out.

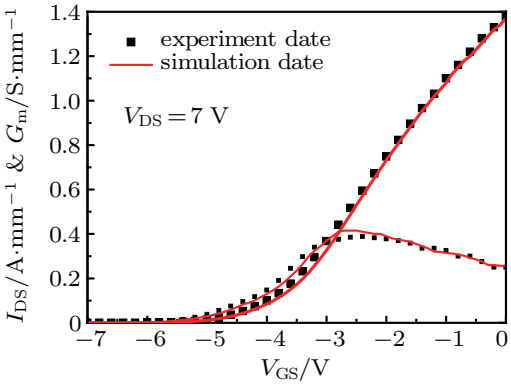


Fig. 2. (color online) Comparison between the measured and simulated transfer characteristics of the conventional HEMT at $V_{\rm DS}=7$ V.

4. Results and discussion

Figure 3 shows the one-dimensional self-consistent simulations of the conduction band energy diagram and electron distribution of the structures with and without an AlInN back-barrier. It is observed that no parasitic electron channel is formed in the back-barrier structure. Comparing with the conventional HEMT, the electron concentration of back-barrier HEMT steeply declines in GaN buffer, which indicates that the 3-nm-thick $Al_{0.64}In_{0.36}N$ layer can significantly enhance the electron confinement. This conduction-band feature is helpful in preventing the carrier from spilling over[25] and the buffer current from leaking. The conduction band edge of $Al_{0.64}In_{0.36}N$ layer at the $Al_{0.64}In_{0.36}N$/GaN interface is about 0.5 eV above the Fermi level. Since the band gap of the $Al_{0.64}In_{0.36}N$ is around 3.44 eV, the valence band edge is well below the Fermi level. Hence, there is no hole accumulation layer forming at this interface.

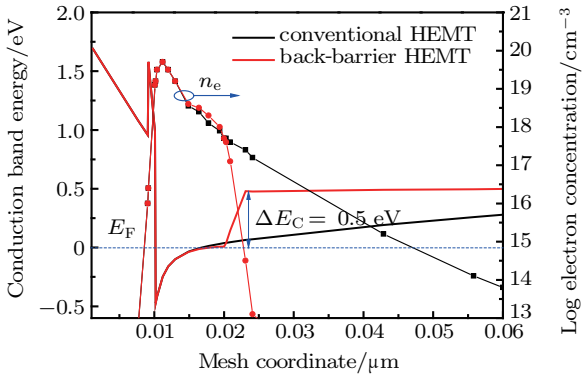


Fig. 3. (color online) Conduction-band energy diagram and the electron distribution in InAlN/GaN structures with and without an AlInN back-barrier.

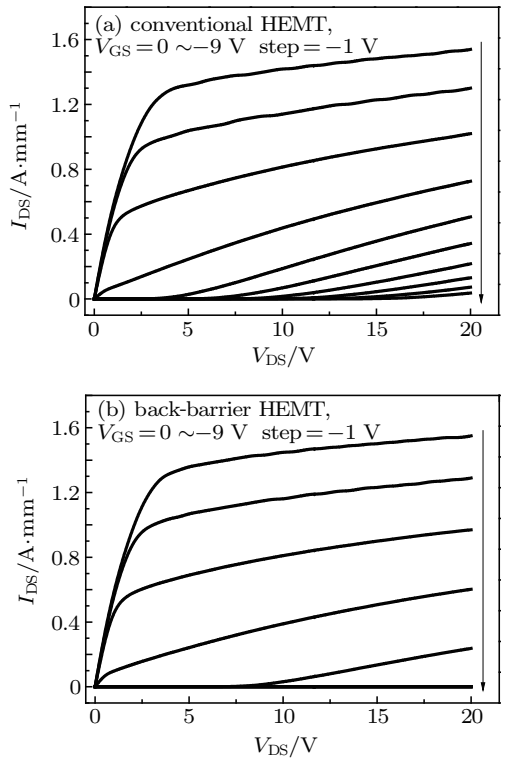


Fig. 4. Simulated *I*–*V* characteristics for (a) conventional HEMT and (b)back-barrier HEMT.

Figure 4 shows the current–voltage (*I*–*V*) characteristics for the two devices. In the back-barrier HEMT, the pinch-off quality is dramatically improved, which relates to the suppression of drain-induced barrier lowering (DIBL). The transfer characteristics of the two devices are plotted in Fig. 5. The threshold voltage of the back-barrier HEMT is about −3.9 V, which positively shifts 1.1 V, compared with the conventional one (−5 V). It is explained by the fact that the opposite polarization field in $Al_{0.64}In_{0.36}N$ layer with respect to that in top barrier layer confines the electrons in a smaller depth range. In the back-barrier HEMT, a peak transconductance of

452 mS/mm is obtained, which is about 10% higher than that achieved in the conventional HEMT at $V_{DS} = 7$ V. Meanwhile, the pinch-off speed is faster than the conventional one due to the steep change of transconductance in the vicinity of pinch-off area, which is essential for better reliability and switching off the transistor. The subthreshold slope (SS) and DIBL values are two major indexes to judge the seriousness of SCE of the device. In the back-barrier HEMT, the DIBL of 82 mV/V is observed as against the 257 mV/V for the conventional HEMT and the SS value of 116 mV/dec is extracted at the steepest point of the transfer curve at $V_{DS} = 7$ V, which is far below the 620 mV/dec obtained in the conventional one. These results indicate that the AlInN back-barrier can effectively suppress the SCE and increase the modulation efficiency of the gate.

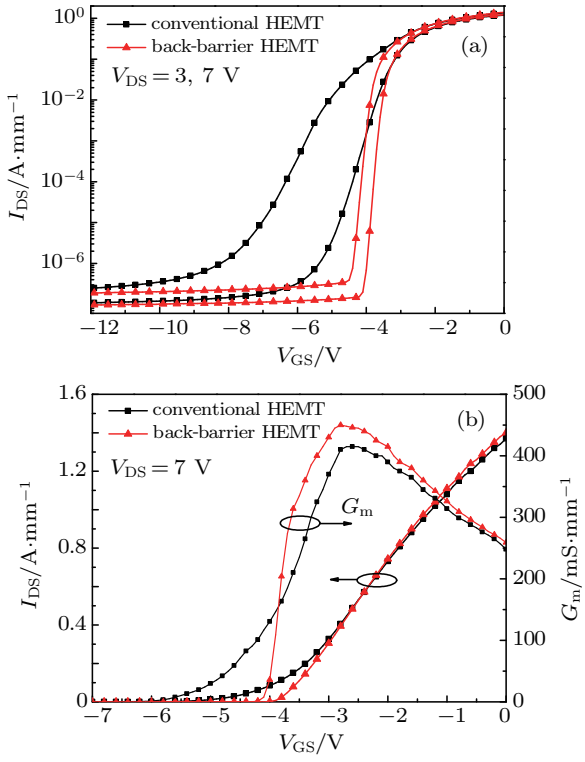


Fig. 5. (color online) (a) I_{DS}–V_{GS} transfer characteristics plotted by the log-scale at $V_{DS} = 3$ V and 7 V for InAlN/GaN HEMTs with and without back-barrier, respectively. (b) G_m–V_{GS} and I_{DS}–V_{GS} transfer characteristics of the two devices at $V_{DS} = 7$ V.

For investigating the ability of the AlInN back-barrier to suppress the SCEs with the gate length scaling down, we simulate the threshold voltages (V_{TH}'s) of HEMTs with and without AlInN back-barrier as a function of gate length (30 nm–200 nm) at $V_{DS} = 7$ V and the results are shown in Fig. 6. In the conventional HEMT, the threshold voltage roll-off becomes obvious, as the gate length is scaled below 100 nm ($t_{bar} = 9$ nm, the thickness of top-barrier layer), which is consistent with the prediction that an aspect ratio (L_G/t_{bar}) greater than ten is needed to keep V_{TH} relatively constant for T-gate device.[26] In the AlInN back-barrier HEMT, as the gate length is shortened to a certain length, the threshold voltage exhibits not so steep roll-off as that of the InGaN back-barrier device in Ref. [17], which may be attributed to the absence of the parasitic electron channel in the AlInN back-barrier layer. In the case of the device with the AlInN back-barrier, no serious SCEs are observed down to 60-nm gate length ($L_G/t_{bar} \approx 6.7$).

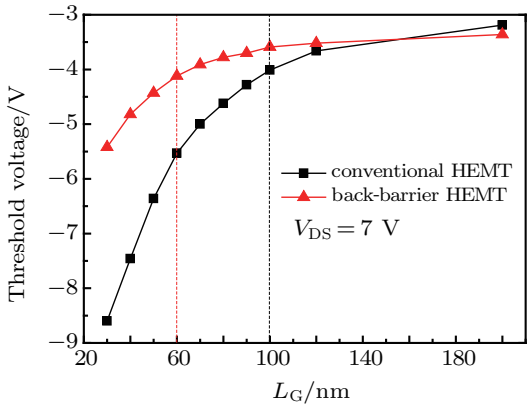


Fig. 6. (color online) Threshold voltages as a function of the gate length of InAlN/GaN HEMTs with and without back-barrier at V_{DS} =7 V, respectively.

The RF device performances of the two devices are also studied by small-signal AC simulation. Figure 7 shows the variations of current gain cutoff frequency (f_T) and power gain cutoff frequency (f_{max}) with gate voltage. A peak f_T of 172 GHz and a peak f_{max} of 217 GHz are obtained in the back-barrier HEMT, which is about 8% higher than that achieved in the conventional HEMT ($f_T = 161$ GHz). The improvement of the peak f_{max} can be observed to be as large as 15%. This improvement results mainly from the increased output resistance.

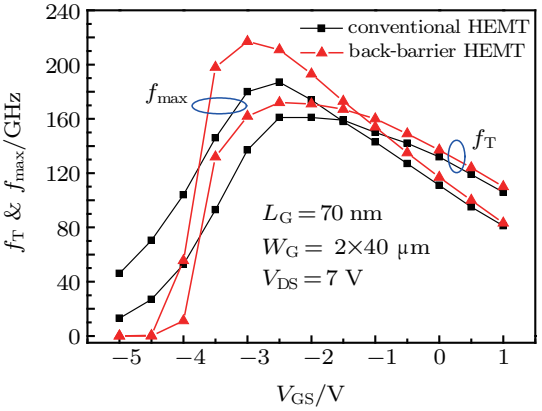


Fig. 7. (color online) Variations of current gain cutoff frequency (f_T) and power gain cutoff frequency (f_{max}) with V_{GS} for the conventional HEMT and back-barrier HEMT at $V_{DS} = 7$ V.

5. Conclusions

In this work, we investigate the influences of a 3-nm-thick $Al_{0.64}In_{0.36}N$ back-barrier on the DC and RF performance of InAlN/GaN HEMT, theoretically. Compared with the conventional InAlN/GaN HEMT, the device with an AlInN back-barrier can significantly enhance the electron confinement and

the modulation efficiency of the gate, which help to suppress the SCEs down to $L_G = 60$ nm (9-nm top barrier). In addition, the back-barrier device also shows distinct improvement on RF performance. So, this new back-barrier material may have great potential to improve the performances of highly scaled devices and the future InN-channel HEMTs. Our study provides a reference for research on AlInN back-barrier application. And, the new back-barrier material may also be conducive to suppressing the current collapse due to the better electron confinement but less total electron density than the conventional devices.

References

[1] Sun H, Alt A R, Benedickter H, Feltin E, Carlin J F, Gonschorek M, Grandjean N and Bolognesi R C 2010 *IEEE Electron Dev. Lett.* **31** 293

[2] Wang R, Saunier P, Xing X, Lian C, Gao X, Gou S, Snider G, Fay P, Jena D and Xing H 2010 *IEEE Electron Dev. Lett.* **31** 1383

[3] Yue Y, Hu Z, Guo J, Sensale-Rodriguez B, Li G, Wang R, Faria F, Fang T, Song B, Gao X, Guo S, Kosel T, Snider G, Fay P, Jena D and Xing H 2012 *IEEE Electron Dev. Lett.* **33** 988

[4] Zhang P, Zhao S L, Xue J S, Zhu J J, Ma X H, Zhang J C and Hao Y 2015 *Chin. Phys. B* **24** 127306

[5] Zhou H, Lou X, Conrad N J, Si M, Wu H, Alghamdi, Guo S, Gordon R G and Ye P D 2016 *IEEE Electron Dev. Lett.* **37** 556

[6] Han T T, Dun S B, Lv Y J, Gu G D, Song X B, Wang Y G, Xu P and Feng Z H 2016 *J. Semicond.* **37** 024007

[7] Uren M J, Nash K J, Balmer R S, Martin T, Morvan E, Caillas N, Delage S L, Ducatteau D, Grimbert B and De Jaeger J C 2006 *IEEE Trans. Electron Dev.* **53** 395

[8] Zervos M, Kostopoulos A, Constantinidis G, Kayambaki M and Georgakilas A 2002 *J. Appl. Phys.* **91** 4387

[9] Bahat-Treidel E, Hilt O, Brunner F, Würfl J and Tränkle G 2008 *IEEE Trans. Electron Dev.* **55** 3354

[10] Lee D S, Gao X, Guo S and Palacios T 2011 *IEEE Electron Dev. Lett.* **32** 617

[11] Meng F, Zhang J, Zhou H, Ma J, Xue J, Dang L, Zhang L, Lu M, Ai S, Li X and Hao Y 2012 *J. Appl. Phys.* **112** 023707

[12] Peng E, Wang X, Xiao H, Wang C, Yin H, Chen H, Feng C, Jiang L, Hou X and Wang Z 2013 *J. Cryst. Growth* **383** 25

[13] Wang C, Zhao M D, Pei J Q, He Y L, Li X D, Zheng X F, Mao Wei, Ma X H, Zhang J C and Hao Y 2016 *Acta Phys. Sin.* **65** 038501 (in Chinese)

[14] Ho S Y, Lee C H, Tzou A J, Kou H C, Wu Y R and Huang J J 2017 *IEEE Trans. Electron Dev.* **64** 1505

[15] Liu J, Zhou Y, Lau K M and Chen K J 2006 *IEEE Electron Dev. Lett.* **27** 10

[16] Palacios T, Chakraborty A, Heikman S, Keller S, DenBaars S P and Mishra U K 2006 *IEEE Electron Dev. Lett.* **27** 13

[17] Lee D S, Gao X, Guo S, Kopp D, Fay P and Palacios T 2011 *IEEE Electron Dev. Lett.* **32** 1525

[18] Kamath A, Patil T, Adari R, Bhattacharya I, Ganguly S, Aldhaheri R W, Hussain M A and Saha D 2012 *IEEE Electron Dev. Lett.* **33** 1690

[19] He X G, Zhao D G, Jiang D S, Zhu J J, Chen P, Liu Z S, Le L C, Yang J, Li X J, Liu J P, Zhang L Q and Yang H 2016 *J. Alloys Compd.* **662** 16

[20] SILVACO Int., 2016 *ATLAS User's Manual, Device Simulation Software* (Santa Clara: CA) p. 2

[21] Ambacher O, Majewski J, Miskys C, Link A, Hermann M, Eickhoff M, Stutzmann M, Bernardini F, Fiorentini V, Tilak V, Schaff B and Eastman L F 2002 *J. Phys.: Condens. Matter* **14** 3399

[22] Pelá R R, Caetano C, Ferreira L G, Furthmüller J and Teles L K 2011 *Appl. Phys. Lett.* **98** 151907

[23] Gonschorek M, Carlin J F, Feltin E, Py, M A, Grandjean N, Darakchieva V, Monemar B, Lorenz M and Ramm G 2008 *J. Appl. Phys.* **103** 093714

[24] He X G, Zhao D G and Jiang D S 2015 *Chin. Phys. B* **24** 067301

[25] Simin G, Hu X, Tarakji A, Zhang J, Koudymov A, Saygi S, Yang J, Khan A, Shur M S and Gsaka R 2001 *Jpn. J. Appl. Phys.* **40** L1142

[26] Jessen G H, Fitch R C, Gillespie J K, Via G, Crespo A, Langley D, Denninghoff D J, Trejo M and Heller E R 2007 *IEEE Trans. Electron Dev.* **54** 2589